Ocean and Coastal Management 187 (2020) 105078

Contents lists available at ScienceDirect

Ocean and Coastal Management

journal homepage: http://www.elsevier.com/locate/ocecoaman

Local land subsidence in Miami Beach (FL) and Norfolk (VA) and its contribution to flooding hazard in coastal communities along the U.S. Atlantic coast

Simone Fiaschi [a,b,*], Shimon Wdowinski [c]

[a] Department of Geosciences, University of Padua, Padua, Italy
[b] Currently at UCD School of Earth Science, University College Dublin, Dublin, Ireland
[c] Department of Earth and Environment, Florida International University, Miami, USA

ARTICLE INFO

Keywords:
InSAR
Land subsidence
Flood hazard
Atlantic coastal communities

ABSTRACT

Increasing rate of sea level rise (SLR) along the US Atlantic coast has resulted in increasing flooding hazard in several coastal communities, including Boston (MA), Norfolk (VA), and Miami Beach (FL). Here, we evaluate the contribution of local land subsidence to coastal flooding hazard in two communities, Miami Beach and Norfolk, using Interferometric Synthetic Aperture Radar (InSAR) time series observations. The InSAR analysis relies on two data sets of ERS-1/2 scenes that were acquired during 1992–1999. The long period covered by the data sets and the large number of available scenes (>20), allowed us to detect movements with lower uncertainty levels (up to 2.4 mm/yr) compared to previous studies. Our results revealed the occurrence of localized subsidence in both communities. In Miami Beach, subsidence at rates of 1–3 mm/yr occurred in a small portion of the territory, mainly in parts of the city built on reclaimed wetlands. In Norfolk, relative subsidence occurred in several localized areas, some along the shore and some inland, at rates of 1–3 mm/yr, while only few sectors show subsidence up to 6 mm/yr. In these areas, the subsidence is higher and reaches ~8 mm/yr if the combined effects of regional-scale (~1.7 mm/yr) and InSAR-derived subsidence is considered. The subsidence observed in this study indicates localized areas of relative higher rate of SLR and a potential increased coastal flooding hazard for both communities.

1. Introduction

The US Atlantic coast is one of the most vulnerable areas to sea level rise (SLR) due to its low elevation, large population concentrations, and economic importance. Many communities along this 3000-km long coastline have been affected by coastal flooding induced mainly by storm surge, high tide, and/or heavy rain. Rising sea level increases the likelihood of such flooding, including rain-induced flooding due to reduced efficiency of gravity-based drainage systems. Over the past decade, several coastal communities, including Boston (MA), Norfolk (VA), and Miami Beach (FL), have experienced increased tidal (nuisance) flooding frequency, which caused significant property damage and disruptions to daily life (Ezer, 2013; Kirshen et al., 2008; Kleinosky et al., 2007; Wdowinski et al., 2016). The long-term rates (>60 years) of relative SLR in Norfolk is 4.6 ± 0.5 mm/yr and in Miami Beach is 2.4 ± 0.4 mm/yr, whereas the decadal-scale rates are faster and are of 5.2 ± 0.6 mm/yr in Norfolk and of 9.0 ± 4.0 mm/yr in Miami Beach (Zervas, 2009; Ezer, 2013; Wdowinski et al., 2016). Rising sea level can also increase the potential damage from storm surge, as in the case of the 2012 "super-storm" Sandy, which took the lives of 185 people and caused property and economic damage of about $65 billion (Aerts et al., 2014).

Vertical land movements (subsidence) can also increase coastal flooding hazard, as it increases the relative rate of SLR. Land subsidence occurs at different scales and can reach rates of more than 200 mm/yr, as observed in Jakarta, Indonesia (Chaussard et al., 2013). The main causes of land subsidence in the tectonically quiescent US Atlantic coast (passive margin) include viscoelastic mantle response to melting glaciers in the Late Pleistocene, ground water extraction, and local sediment compaction. The regional-scale subsidence due to mantle flow, termed Glacial Isostatic Adjustment (GIA), affects the Atlantic coast from New Hampshire to northern Florida (Karegar et al. 2016, 2017; Sella et al.,

* Corresponding author. Department of Geosciences, University of Padua, Padua, Italy.
E-mail address: simone.fiaschi@ucd.ie (S. Fiaschi).

https://doi.org/10.1016/j.ocecoaman.2019.105078
Received 26 September 2019; Received in revised form 8 December 2019; Accepted 17 December 2019
Available online 26 December 2019

2007). Basin-scale subsidence has occurred in various locations along the mid-Atlantic coastal plain, including the southern Chesapeake Bay region and along the Carolina coasts due to massive groundwater extraction (Eggleston and Pope, 2013). Local-scale land subsidence occurs in many locations along coastal areas, especially in sediment rich areas, such as river deltas, and reclaimed land and wetlands. For example, land subsidence in New Orleans occurred mainly in new neighbourhoods built on reclaimed wetlands (Dixon et al., 2006).

Coastal subsidence along the US Atlantic coast has been estimated by both geological and geodetic methods and found to be in the range of 0–4 mm/yr. Geologically-based subsidence rates were determined from late Holocene (past 4000 years) sediment records in various coastal locations and found to be in the range of 0–2 mm/yr (Engelhart and Horton, 2012; Karegar et al. 2016, 2017; Kemp et al., 2014; Nikitina et al., 2015). The geological rates reflect the long-term subsidence components of sediments compaction and GIA. Geodetic observations acquired by levelling, extensometers, and Global Positioning System (GPS) provide direct measurements of the present-day subsidence rate. Throughout most of the Atlantic coast, the geodetic and geologic determined rates are similar, except along a section of the mid-Atlantic coast between Virginia and South Carolina (32.5–38°N), where present-day geodetic rates reach 4 mm/yr, about double the long-term geologic rate (Karegar et al., 2016). The high subsidence rate in the mid-Atlantic region is attributed to aquifer system deformation in response to massive groundwater extraction, which began in the turn of the 20th century, but has intensified since the 1960's (Eggleston and Pope, 2013; Karegar et al., 2016) (Fig. S1). The geodetically observed subsidence rates along the US Atlantic coast are based on GPS and/or extensometers point measurements located tens of kilometres from one another. Thus, these measurements provide the long wavelength (>50 km) characterization of coastal subsidence, but are limited in detecting shorter wavelength subsidence, for example occurring by sediment compaction. A recent Interferometric Synthetic Aperture Radar (InSAR) analysis of ALOS-1 data acquired during 2007–2011 over the Hampton Roads, which also includes the city of Norfolk, VA, detected localized deformation patterns (<100 m) in that area, but revealed limited results due to the short length of the time series (Bekaert et al., 2017).

In this study, we use InSAR time series acquired by the ERS-1/2 satellites during 1992–1999, to detect localized subsidence in two coastal communities, Miami Beach and Norfolk (Fig. 1A). Both communities have been subjected to repeated coastal flooding over the past decade (Ezer, 2013; Wdowinski et al., 2016). In Miami Beach flooding has occurred mostly in the western part of the city, west of Alton Road (Fig. 1B), which was constructed on reclaimed wetland (Wdowinski et al., 2016). In Norfolk, flooding has occurred in multiple locations throughout the city characterized by low elevation (Fig. 1C). Our study relies on 6-7 year-long ERS-1/2 observations, which are significantly longer than the 4-year long ALOS-1 observations used previously to study land subsidence in the Norfolk area (Bekaert et al., 2017). The longer observation period and the larger number of available SAR scenes enable us to detect small vertical movements with almost half the uncertainty level compared to the shorter time series of the previous study (Havazli and Wdowinski, 2017). The high spatial resolution of the InSAR observations (~20 m by 20 m) is capable of detecting the distribution and rate of localized subsidence in both study areas and, consequently, providing better local-scale assessments of coastal flooding hazards for

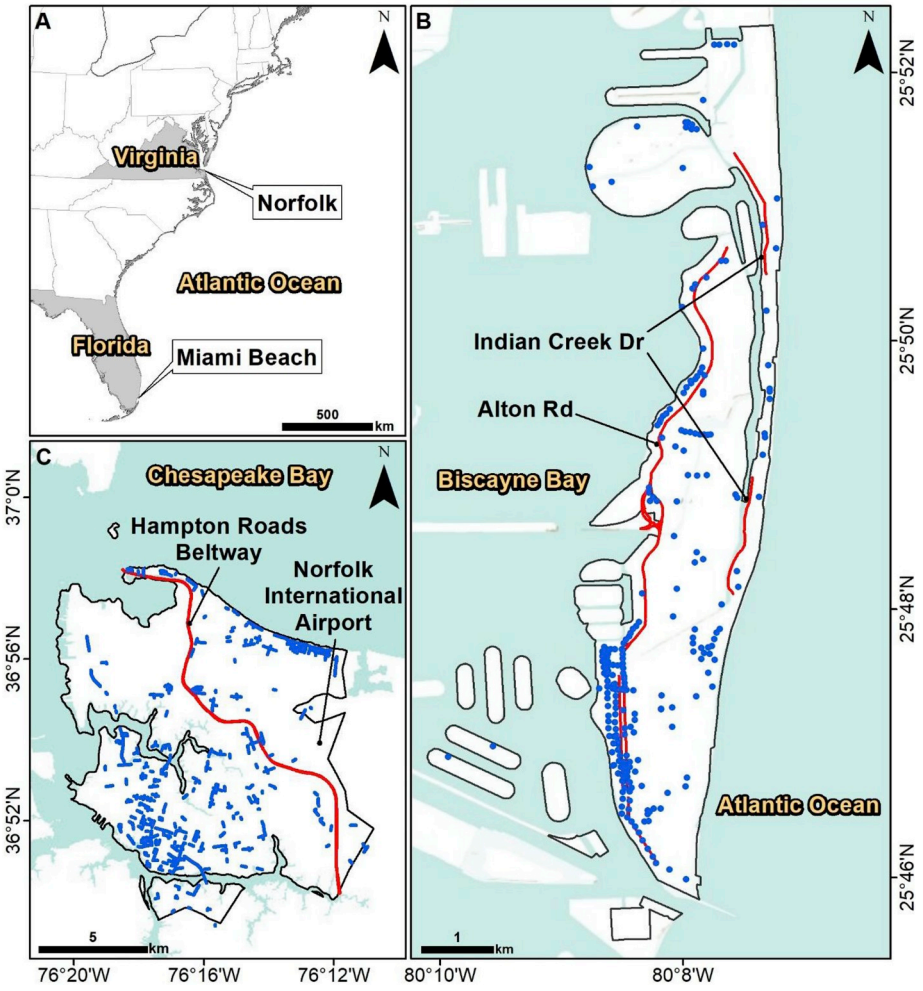

Fig. 1. Location of the study areas. (**A**) Map of the US Atlantic coast showing the locations of Miami Beach and Norfolk (VA); (**B**) Flood affected areas in Miami Beach. Blue dots mark the locations of the claimed rain and high tide flooding events during 1998–2012. Red lines mark the location of roads affected by flooding during the same time period (data from Wdowinski et al., 2016). (**C**) Norfolk (VA), the blue lines are the streets and intersections reported as flooded in storm from 9/30/2010 to 05/01/2015 (data from http://va-norfolk.civicplus.com). The red lines mark the location of the main roads discussed in the text. Base image source: Esri, DigitalGlobe, GeoEye, Earth Geographics, CNES/Airbus DS, USDA, USGS, AeroGRID, IGN, and the GIS User Community. (For interpretation of the references to colour in this figure legend, the reader is referred to the Web version of this article.)

both communities.

2. Available data sets

Results were obtained from two sets of C-band (5.6 cm wavelength) SAR scenes acquired by the ERS-1/2 satellites, which are available from the European Space Agency (ESA) archive. The first data set, covering the Miami Beach area, consists of 24 scenes acquired from 03/05/1993 to 06/05/1999 (Table S1); the second, covering the city of Norfolk, consists of 32 scenes acquired from 19/06/1992 to 09/11/1998 (Table S2). Both sets of images have been acquired with average look angle of 23°, heading angle of 193° and revisit time of 35 days. It must be noted that, even if the minimum revisit time of the ERS-1/2 satellites is 35 days, the temporal distribution of the SAR scenes is not uniform and gaps up to two years are present in both data sets (Tables S1 and S2). The nominal pixel spacing is 7.90 m in slant range and 3.98 m in azimuth. The ERS-1/2 data extend over a relatively long-time span (6–7 years) and contain sufficient number of scenes (>20) needed to reach measurement accuracy of 1–2 mm/yr (Havazli and Wdowinski, 2017). Other satellites missions (ALOS-1/2, RADARSAT-1/2, ENVISAT) did not acquire a sufficient number of scenes along the US Atlantic coast or acquired data over a shorter time period and, hence, cannot provide the accuracy required for our study.

3. Methods

The two ERS-1/2 data sets were processed using the Small Baseline Subset (SBAS) algorithm (Berardino et al., 2002) as implemented in the SARscape modules (software version 5.2.1) available under ENVI platform (software version 5.3). For the Miami Beach study area, 95 interferometric pairs were connected by setting the maximum perpendicular and temporal baselines respectively to 55% (relative to the critical baseline value, Table S3) and 1,000 days (Fig. 2A). For the Norfolk study area, 182 interferometric pairs were connected by setting the baselines to 60% (relative to the critical baseline value, Table S4) and 1,200 days (Fig. 2B). A multi-look factor of 1 in slant range and 5 in azimuth directions was applied to obtain a ground pixel resolution of ~20 m by 20 m. The interferometric phase related to the topography was removed using the 1 arc-second Shuttle Radar Topography Mission (SRTM) DEM. Orbital inaccuracies are compensated by using ESA's Precise Orbits (PRC) data. Spectral shift and common Doppler bandwidth filtering are applied during the interferogram generation to minimize decorrelation effects (Gatelli et al., 1994). The noise and signal frequencies are smoothed in a selective way by using the Goldstein adaptive filter (Goldstein and Werner, 1998). The filter strength is based on the local coherence and is controlled by the "α" parameter that was set to 0.3–1.0 (minimum values) and 2.5–3.0 (maximum values) respectively for Miami Beach and Norfolk. The interferograms are co-registered to the geometry of a master image and unwrapped using the Delaunay Minimum Cost Flow (MCF) algorithm (Costantini, 1998). An unwrapping coherence threshold of 0.30 was set for both data sets. Residual orbital inaccuracies, phase offsets and/or phase ramps are removed by using a cubic polynomial refinement on selected ground control points (Figs. S2 and S3). The ground control points used in this study are not calibrated with ground velocities obtained with other geodetic methods such as GPS, and hence the produced maps of relative subsidence do not take into account any regional-scale deformation. The residual height correction factors and the average displacement rates are retrieved by inverting a linear system via the Singular Value Decomposition (SVD) method (Strang, 1988). The Atmospheric Phase Screen (APS) is then calculated and removed by applying spatial (low-pass) and temporal (high-pass) filters. The corrections are carried out assuming that the atmospheric phase delays are correlated in space and uncorrelated in time (Emardson et al., 2003). For both data sets, the low-pass and high-pass filters were set respectively to 1200 m and 365 days. The final products consisting of mean velocities and displacements time series are calculated and geocoded to the WGS 1984 UTM Zone 17N (Miami Beach) and 18N (Norfolk) projected coordinate system. During the SBAS processing chain the multi-temporal coherence is estimated for each pixel by evaluating the interferometric correlation in the entire interferograms stack. The coherence $|\gamma|$ between two coregistered complex SAR images y_1 and y_2 is calculated as the maximum likelihood estimator of the coherence magnitude over an estimation window of N pixels (Seymour and Cumming, 1994)

$$|\gamma| = \frac{\left|\sum_{n=1}^{N} y_1^{(n)} y_2^{*(n)}\right|}{\sqrt{\sum_{n=1}^{N} |y_1^{(n)}|^2 \sum_{n=1}^{N} |y_2^{(n)}|^2}} \quad 0 \le |\gamma| \le 1$$

The multi-temporal coherence (denoted as γ for simplicity) can be used as a measure of the accuracy of the interferometric phase (Hanssen, 2001). The relative uncertainty (σ) (Sarmap, 2014) of the mean InSAR-derived velocities is then internally calculated for each pixel as (simplified from: Bamler and Just, 1993)

$$\sigma = \frac{\lambda}{4\pi} \sqrt{\frac{1-\gamma^2}{2\gamma^2}}$$

where λ is the signal wavelength. The obtained uncertainty values are between 0.2 mm/yr and 1.5 mm/yr (mean value of 0.6 mm/yr) for Miami Beach (Fig. S4), and between 0.1 mm/yr and 2.4 mm/yr (mean value of 0.6 mm/yr) for Norfolk (Fig. S5). Assuming that the ground movements in both study areas do not present strong horizontal components, the mean LOS velocities are projected to the vertical direction taking into account the incidence angle of each measured point. The final results were classified in a Geographic Information System (GIS) (ArcGIS 10.6 software) using a colour scale from blue to red, in which positive values, in blue, correspond to a decrease of the sensor to target slant range distance (i.e. relative uplift), while negative values, in red, correspond to an increase of the sensor to target slant range distance (i.e. relative subsidence). The points considered as stable, in green, are the ones with velocities of ±1 mm/yr, close to the accuracy obtainable with the ERS-1/2 satellites (Crosetto et al., 2008).

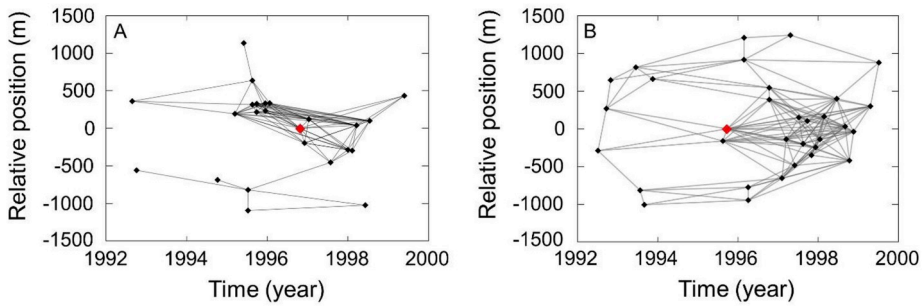

Fig. 2. SBAS connection networks. Interferometric pairs generated for (**A**) Miami Beach from 1993 to 1999 and (**B**) Norfolk (VA) from 1992 to 1998. The red dots are the images used as master. (For interpretation of the references to colour in this figure legend, the reader is referred to the Web version of this article.)

4. Results

Miami Beach is a densely populated barrier island, located between Biscayne Bay and the Atlantic Ocean (Fig. 1b). It is roughly 10 km long and 2.5 km wide at its widest point. InSAR time series results reveal a patch-like pattern of coherent velocity observations, reflecting contributions from variable scattering environments and high variability of tropospheric delay. Coherent results occur over the built environment, whereas incoherent results occur over open areas and some of the built environment. The point density obtained with the SBAS approach is of 924 points/km^2. Among the 18,949 measured points, 1555 present velocities below −1.0 mm/yr, while only 11 of them have velocities below −3 mm/yr (Table S5). The results indicate that most of the city (~97%) was stable during the 1993–1999 observation period (green in Fig. 3A). However, several localized subsiding areas were detected mostly in the western part of the city (yellow in Fig. 3A). These areas typically consist of single-family houses that were built on reclaimed wetlands (e.g. southernmost black circles in Fig. 3A). In some locations, as in the eastern part of the city, the detected subsidence is of a 12-story high condominium building (northernmost black circle in Fig. 3A). The detected subsidence rate is in the 1–3 mm/yr range, with uncertainty level of 0.6–0.8 mm/yr. Although higher subsidence velocities up to 3.8 mm/yr are registered in the artificial islands located west of the city, phase unwrapping errors leading to higher uncertainties cannot be excluded in such areas.

The city of Norfolk, Virginia, is located in lower Chesapeake Bay, which is the largest estuary in the U.S (Fig. 1A). The city is surrounded by water from the Bay in the north and secondary rivers and estuaries in the west and south (Fig. 1C). Since the entire Chesapeake Bay area is subject to regional subsidence, the results obtained from the SBAS InSAR processing over Norfolk are the expression of the differential movements of the measured points relative to the subsiding land surface. To obtain the total subsidence in the area, the contribution of the regional subsidence obtained from GPS observations from 2009 to 2017 (1–2.4 mm/yr) (Bekaert et al., 2017) must be added to the InSAR measurements. The InSAR analysis over Norfolk extends well beyond the city limits (Fig. 4) and covers also the nearby GPS sites. However, the results here reported refer, unless otherwise specified, only to the area of the municipality (Fig. 1C). Thanks to the SBAS technique, we obtained very high point density (2140 points/km^2) and covered almost the entire territory of Norfolk, except for the areas characterized by very low coherence corresponding to water bodies and dense vegetation (Fig. 4). The results, show that most of the city lies over a relatively stable territory while only few localized areas are affected by subsidence up to 6.0 mm/yr. Among the 313,052 measured points, 74,831 registered subsidence greater than 1.0 mm/yr (24%), and only 1106 greater than 3 mm/yr (0.3%). Four main locations are here reported as examples of localized subsidence in the Norfolk area (Figs. 4 and 5): A) Willoughby Spit and tunnel island; B) Craney Island and Lamberts Point terminal; C) East Beach residential area; D) Hampton Road Beltway. The extent of the subsiding areas is generally limited to localized residential or industrial sites; only in the case of Norfolk International Airport and its surroundings the subsidence extent is larger (Fig. 5D). Subsidence in this area also intersects the Hampton Road Beltway for a total length of around 6000 m. In the four selected locations, most of the subsiding points registered velocities between −1.0 mm/yr and −3.0 mm/yr, while only a smaller percentage had higher subsidence rates, up to −6.0 mm/yr (Table S6). The measurement uncertainties are in the range of 0.1–2.4 mm/yr.

A section of the Hampton Roads Beltway close to the Norfolk International Airport shows subsidence rates ranging from 1.0 mm/yr to 4.0 mm/yr (Fig. 5D). Outside the study area, around 9 km west of the Norfolk city limits, another 4000 m long section of the Hampton Road Beltway is affected by higher subsidence rates up to 8.3 ± 1.0 mm/yr (Fig. 4). Localized subsidence occurred also in the East Beach residential area (Fig. 5C), north of the city. Here, the subsidence rates can reach 3.3 mm/yr. Similar rates of subsidence affected Willoughby Spit in the northern section of the city, whereas the west flank of the man-made

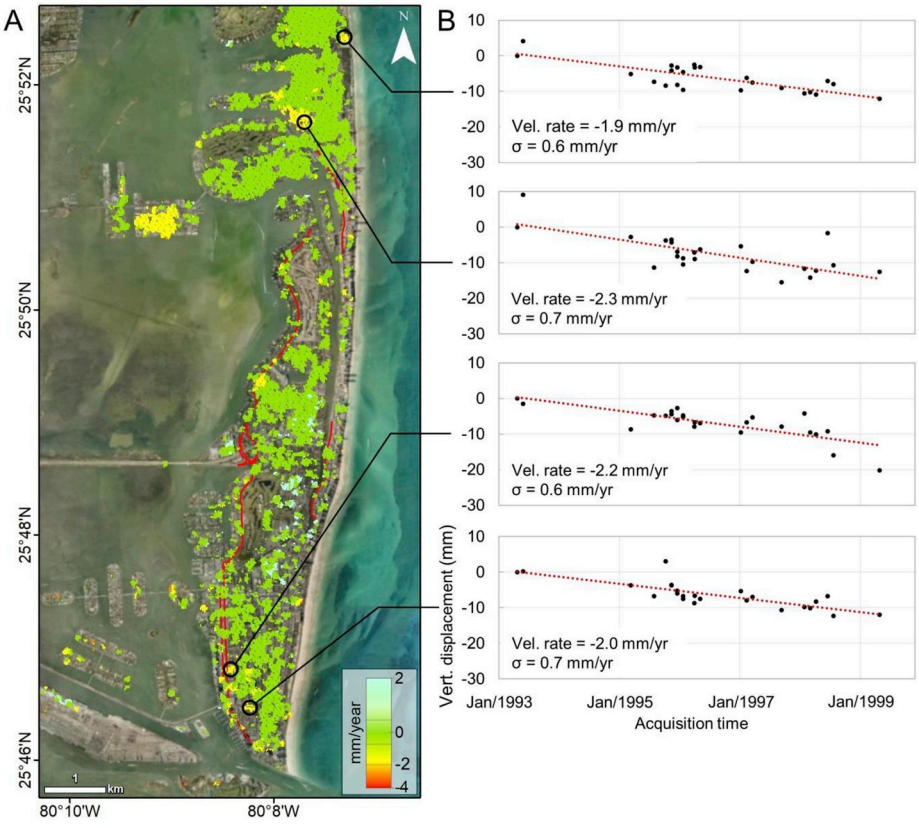

Fig. 3. Vertical velocity map over Miami Beach from 1993 to 1999 and displacement time series. (**A**) vertical velocity map obtained with the SBAS technique. The black circles mark the location of the extracted displacement time series. Red lines mark the location of roads affected by flooding during 1998–2012 (data from Wdowinski et al., 2016). (**B**) Vertical displacement time series of the four selected points. Base image source: Esri, DigitalGlobe, GeoEye, Earth Geographics, CNES/Airbus DS, USDA, USGS, AeroGRID, IGN, and the GIS User Community. (For interpretation of the references to colour in this figure legend, the reader is referred to the Web version of this article.)

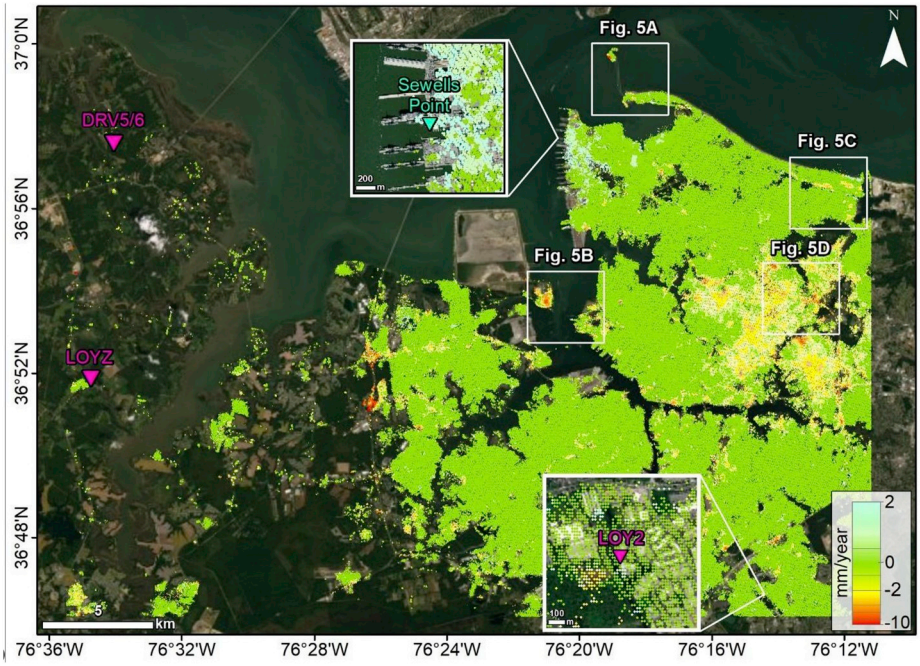

Fig. 4. Vertical velocity map over Norfolk (VA) from 1992 to 1998. The white squares are the locations of the four areas affected by land subsidence reported in Fig. 5. Purple triangles are the locations of the GPS stations available in the area. The light blue triangle is the location of the Sewells Point tide gauge station. Base image source: Esri, DigitalGlobe, GeoEye, Earth Geographics, CNES/Airbus DS, USDA, USGS, AeroGRID, IGN, and the GIS User Community. (For interpretation of the references to colour in this figure legend, the reader is referred to the Web version of this article.)

island at the entrance to the Hampton Roads Bridge–Tunnel (HRBT) registered subsidence up to 6.3 mm/yr (Fig. 5A). Subsidence up to 4.1 mm/yr affected also parts of the Lamberts Point coal terminal, whereas the subsidence is more evident in the near Craney Island where the entire Oily Waste Treatment Plant subsided with rates reaching 5.1 mm/yr (Fig. 5B). The analysis of the displacement time series extracted in the four main areas (Fig. 5), shows a similar deformation trend that appear to be linear in each of the selected points. The non-uniform temporal distribution of the images, with a gap of information between 09/1993 and 04/1995, and the production of decorrelation effects can explain the occurrence of anomalous displacement values that are visible, for example in P4.

5. Discussion

InSAR time series analysis of the two coastal communities, Miami Beach and Norfolk, reveals that during the observation period of 1992–1999, both communities were subjected to localized differential subsidence at rates of 1–3 mm/yr in Miami Beach and 1–6 mm/yr in Norfolk. In Miami Beach, subsidence is limited to several small areas (~3% of the analysed area; Fig. 3), mostly located in the western side of the city, which was built on reclaimed wetlands. The rest of the city remained stable, which agree with the two years of continuous GPS observations in Miami Beach (Station: FLMB) and four other station locations in southeast Florida. The geology of the area is, in fact, constituted by a plateau of karst limestone (Miami Limestone Formation) sitting over the Florida Platform (Lane, 1994). Although no regional subsidence has been recorded in south Florida, localized subsidence can occur as consequence of karst activity and compaction of unconsolidated sediments. In Norfolk, differential subsidence occurred over wider areas (~20% of the municipality), as wide as 7–8 km, but also in smaller areas with dimension of tens to hundreds of meters (Figs. 4 and 5). Subsidence affected also critical infrastructure such as the Hampton Road Beltway (Fig. 5D). This road is one of the main designated hurricane evacuation routes for people in vehicle to flee the Virginia Beach (East of Norfolk) and Norfolk areas, as reported from the Virginia Department of Emergency Management. The presence of subsiding areas along the route may increase the flooding hazard in case of storm surges and can be a significant aspect to be considered by the Authorities for planning evacuation strategies. Our Miami Beach results are first to report land subsidence in the city. However, land subsidence in Norfolk was reported previously, both in term of regional component (Karegar et al. 2016, 2017) and localized differential component (Bekaert et al., 2017). Although most of Norfolk seems stable (green in Fig. 4), the entire city subsides at a rate of 1.5–2.5 mm/yr as part of the GIA process (Bekaert et al., 2017; Karegar et al. 2016, 2017). Thus, we added the regional component derived from the LOY2 GPS during 02/2009–04/2017 (−1.7 ± 0.9 mm/yr) to our observed relative subsidence (1–6 mm/yr) and presented it in Fig. S6.

The previous study of Bekaert et al. (2017) used GPS observations in the lower Chesapeake Bay area to calibrate their InSAR results, which were derived from ALOS-1 observations acquired during 2007–2011. Their results revealed a very diffuse subsidence pattern occurring throughout most of the city with rates ranging 0–10 mm/yr. However, the limited number of SAR data and the 4-year observation period used in their study yielded very high uncertainty rates (5–8 mm/yr), which were not sufficient for generating accurate subsidence maps (Bekaert et al., 2017). Our results, however, rely on more observations and a longer acquisition period (6–7 years) and, hence, yielded a more accurate subsidence map (uncertainties up to 2.4 mm/yr) showing localized subsidence patterns.

Localized subsidence typically occurs in response to shallow subsurface processes as sediment compaction, often in response to groundwater extraction (Amelung et al., 1999; Galloway and Burbey, 2011), and soil settlement in reclaimed areas (e.g., Kim et al., 2008). The rate of localized subsidence can vary over time, depending on the controlling mechanisms. Subsidence rate due to groundwater exploitation is affected by extraction and recharge histories, as well as by the deformation characteristics of the aquifer system. Subsidence rate due to soil settlement in reclaimed areas also varies in time, as the rate of soil compaction decreases over time. Despite the time dependent nature of localized subsidence, it can be characterized by linear rates, as presented in this study, reflecting a mean, uniform rate of subsidence that occurred during the observation period. The application of the observed rates beyond the observation periods is a good first assumption, as the deformation processes tend to vary at slow rates, especially if no other observations are available. However, the extension of the observed subsidence rates beyond the observation period should be done with

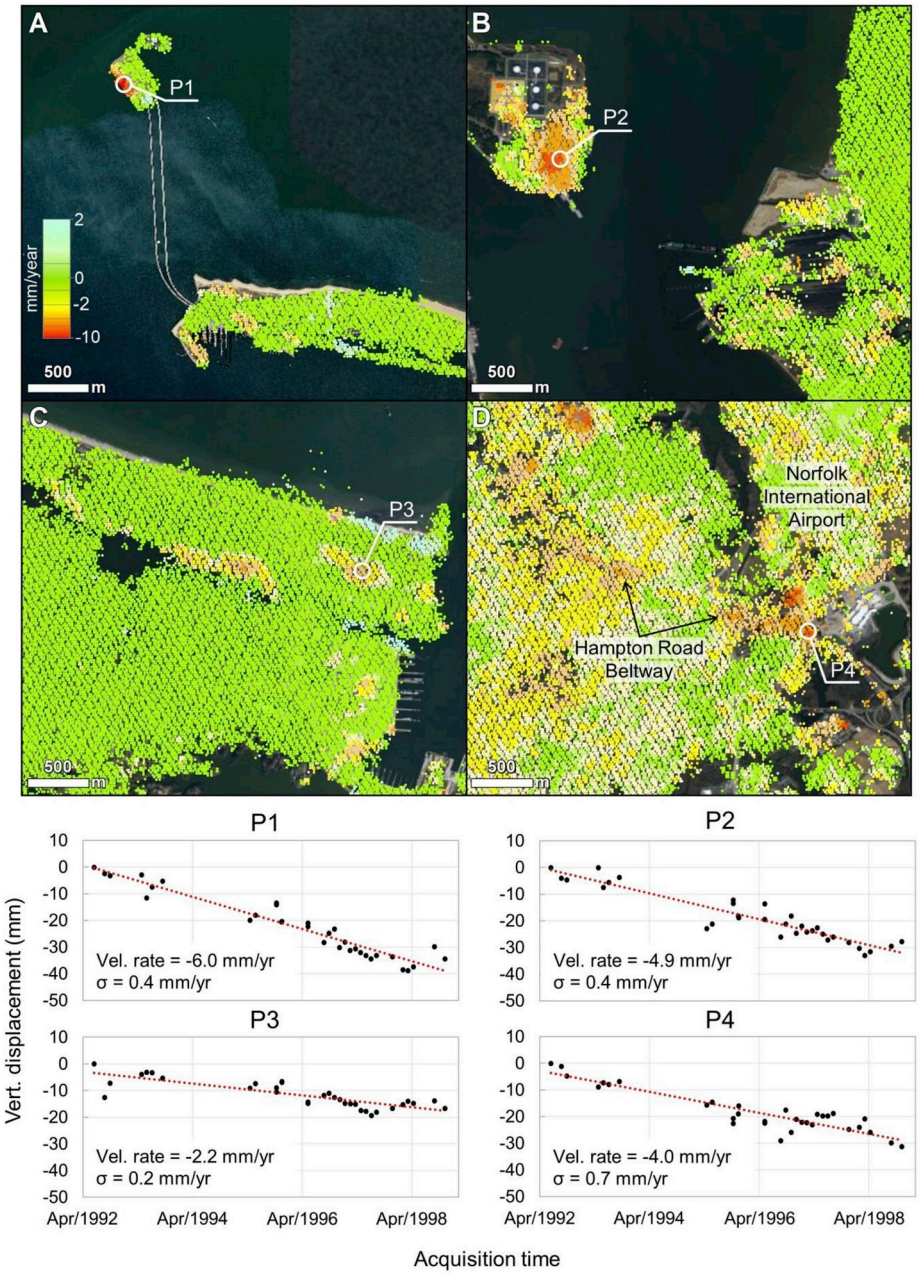

Fig. 5. Main areas affected by subsidence in Norfolk (VA). (**A**) Willoughby Spit and tunnel island. (**B**) Craney Island (left) and Lamberts Point terminal (right). (**C**) East Beach residential area. (**D**) Hampton Road Beltway. The white circles mark the location of the extracted displacement time series. (**P1–P4**) Vertical displacement time series extracted from four selected points in Norfolk (VA). Base image source: Esri, DigitalGlobe, GeoEye, Earth Geographics, CNES/Airbus DS, USDA, USGS, AeroGRID, IGN, and the GIS User Community.

caution.

The high spatial resolution of InSAR time series analysis can be used to evaluate stability of buildings, as well as point measurement of geodetic instruments, such as continuous GPS stations or tide gauges, as previously done in the Venice Lagoon (Italy) (Bock et al., 2012) and in Berst (France) (Poitevin et al., 2019). Here, we use the InSAR-derived relative velocity map of Norfolk to evaluate the stability of the Sewells Point tide gauge, which is used to estimate the rate of relative SLR for Norfolk, and the LOY2 continuous GPS station (Fig. 4), which is used to estimate the regional land subsidence component (1.7 ± 0.9 mm/yr). Unfortunately, we were unable to evaluate the stability of the LOYZ and DRV5/6 GPS stations (which measure regional land subsidence respectively of 1.8 ± 0.8 mm/yr and 1.9 ± 0.5 mm/yr), because both stations are surrounded by vegetated areas, which do not maintain sufficient interferometric coherence in the C-band ERS-1/2 data to obtain reliable results. We are also unable to directly determine the stability of the Sewells Point tide gauge, as the gauge is located at the end of a peer, which does not provide a good scattering environment and shows patchy areas of slight uplift (insert in Fig. 4). However, the scatterers located within the broader area of the Naval Base indicate relative stability of the area (average movement rate of 28,401 points is 0.5 ± 0.6 mm/yr). After correcting the relative InSAR subsidence field by the regional subsidence component of ~1.7 mm/yr (Fig. S6), the Naval Base exhibits an average subsidence rate of ~1.2 mm/yr, which explains the high relative SLR at Sewells Point (4.6 ± 0.3 mm/yr) compared to the global mean SLR (3.2 ± 0.3 mm/yr). Our results also indicate that the LOY2 GPS station is stable based on statistical analysis of 18 InSAR points found within 50 m buffer distance from the GPS station revealing relative average motion of 0.4 ± 0.4 mm/yr.

We did not conduct a similar stability analysis for Miami Beach, because no tide gauge or GPS stations were operating in the study area during the ERS-1/2 measurement period. The Miami Beach tide gauge operated during the years 1931–1981 and then was relocated to Virginia Key in 1994. The one continuous GPS station operating in Miami Beach

(FLMB) started operation in 2017 and, insofar, its record indicates no measurable subsidence.

Coastal flooding hazard assessments often rely on the rate of relative SLR for forecasting inundation level and/or flooding frequencies in coastal communities. For example, Burgos et al. (2018) calculated future nuisance flooding frequency in Norfolk using rate of relative SLR of 4.6 ± 0.3 mm/yr derived from the 1927–2016 Sewells Point's tide gauge record. These results are representative for most of the city, but not for areas subjected to localized subsidence. In those areas the rate of relative SLR is higher and can reach level of 8–9 mm/yr, according to the obtained results. In particular, localized subsidence may naturally occur in low elevation areas that are more vulnerable to flooding. Based on a LiDAR DEM acquired in 2013, we calculated that 614 of the total subsiding points in the Norfolk municipality lie at an elevation <1 m above North American Vertical Datum of 1988 (NAVD88), which is < 1.08 m above Mean Sea Level. These 614 points represent an area of ~25 ha (0.17% of the territory) in which the flooding hazard can be higher due to the combination of local subsidence and low elevation. In Miami Beach, some of the localized subsiding areas are located hundreds of meters inland of the shoreline (Fig. 3), suggesting a negligible contribution for increasing the rate of relative SLR at these sites. However, these localized subsiding areas can increase the likelihood of rain-induced flooding, which occur during heavy rain events. The comparison between the InSAR results and the flooding events reported between 1998 and 2015 (Fig. 6) shows that 59% and 30% of the detected subsiding points in Miami Beach and Norfolk municipalities, respectively, are within 200 m of areas already subjected to flooding. This suggests that a contribution of the detected subsidence to the more recent flooding events in these areas is possible, but further and more recent data are required to confirm such statement.

In the current study, we used ERS-1/2 data acquired during a 7-year long period, which allow us to obtain results with uncertainty lower than 1 mm/yr in most areas (Figs. S4 and S5). However, in some locations, uncertainty reached 2–3 mm/yr level, suggesting caution in the evaluation of the velocities in these areas. Another issue that can limit the significance of our results is nature of the measured objects on the surface. SAR measurements in urban areas are dominated by double-bounce backscattering from buildings (Hong and Wdowinski, 2014; Yamaguchi et al., 2005) and, hence, represent mainly building movements. Thus, subsiding areas with stable buildings, which are anchored at depth by piling to a stable stratum, will reveal in InSAR analysis as stable, non-subsiding surface conditions. As an example, such differential subsidence behaviour was detected in Mexico City indicating apparent uplift of large, well anchored building or structures, as Metro stations, with respect to their surroundings (Osmanoglu et al., 2011; Solano-Rojas et al., 2019). Therefore, our reported subsidence results may represent movement of buildings and not of the actual surface.

Here we focused on Miami Beach and Norfolk because both have been subjected in the past couple of decades to increased frequency of nuisance flooding, which caused property damage and affected daily life. However, the importance of our study extends well beyond these two coastal areas, because similar deformation processes affect many other coastal communities. With the projected increase of sea level, additional communities along the US Atlantic coast and in other coastal areas worldwide will be subjected to more frequent nuisance flooding. Thus, improved management of coastal flooding hazard in most coastal communities should take into account studies and assessments of vertical land movements, which include contributions from both regional and local land subsidence. The regional component is best evaluated using GPS measurements, whereas the local subsidence is best measured with InSAR in urban areas and GPS in open areas. Thus, future assessments of coastal flooding hazards should include measurements and analyses of both GPS and InSAR data. Recently, the state of Florida initiated a coastal subsidence monitoring project in Miami-Dade County, which implements the recommended dual GPS-InSAR monitoring approach.

Our InSAR time series analysis has some limitations in terms of observation period and measurement uncertainty. Our results are based

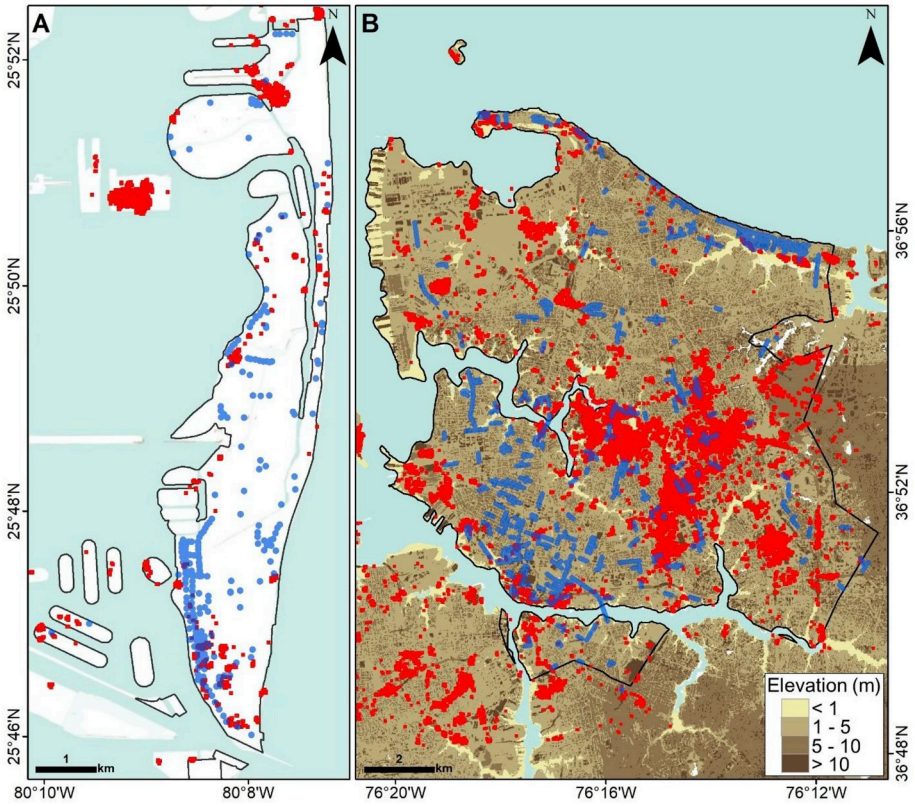

Fig. 6. Comparison between areas affected by subsidence detected with InSAR (vertical velocity < −1 mm/yr, red) and the flooding reported (blue) in Miami Beach (data from Wdowinski et al., 2016) (**A**) and Norfolk (data from http://va-norfolk.civicplus.com) (**B**) municipalities. Data in (**B**) are superimposed to the LiDAR elevation map (NAVD88). Base image source: Esri, DigitalGlobe, GeoEye, Earth Geographics, CNES/Airbus DS, USDA, USGS, AeroGRID, IGN, and the GIS User Community. (For interpretation of the references to colour in this figure legend, the reader is referred to the Web version of this article.)

on ERS-1/2 data acquired more than two decades ago and, hence, reflect localized subsidence occurred during the observation time period (1992–1999). As explained above, the application of the observed rate beyond the observation period should be done with caution. Unfortunately, follow up SAR missions, as ENVISAT and ALOS-1, did not acquire a sufficient number of images over the US Atlantic coast to obtain reliable velocity observations needed for assessing coastal subsidence at the 1–2 mm/yr uncertainty level. The currently operating Sentinel-1 mission acquires SAR data over the US Atlantic coast in a systematic manner since 2016. The currently available Sentinel-1 data expand over a period of three years, which is still not sufficient to detect surface movements at the desired 1–2 mm/yr uncertainty level (Havazli and Wdowinski, 2017). However, this uncertainty level will be reached as soon as Sentinel-1 acquisitions will cover a period greater than four/five years (Havazli and Wdowinski, 2017). Considering the great potential of Sentinel-1 data to detect ground movements over large scales at improved resolution in comparison with past-generation satellites, future work will consist in upscaling this study to a larger number of communities along the US Atlantic coastline, and assessing the contribution of the more recent land subsidence to flooding hazard in such areas.

6. Concluding remarks

In this study, SAR images acquired by the ERS-1/2 satellites between 1992 and 1999 are used to measure local land subsidence in two communities located along the US Atlantic coastline, Miami Beach (FL) and Norfolk (VA). Both communities have been affected by increasing frequency of flooding events, in Miami Beach mainly due to increasing rate of sea level rise, while in Norfolk mainly due to regional subsidence as consequence of GIA and groundwater exploitation. Our InSAR results show that in both communities land subsidence contributes locally to higher relative sea level rise rates. In Miami Beach, land subsidence occurred only locally and at very low rates, between 1 mm/yr and 3 mm/yr. In Norfolk, land subsidence affected a larger portion of the territory with rates up to 6 mm/yr (8 mm/yr if considering both relative and regional components). This study shows the importance of considering land subsidence as one of the principal factors that affect the spatial distribution of flooding events and their frequency in low-lying coastal communities. The information provided by the InSAR analysis are valuable to local authorities for improving flood hazard assessments and for helping the development and implementation of more efficient flood emergency response and recovery plans.

Although this study provides an unprecedented overview of the land motion occurring in the Miami and Norfolk communities, our InSAR results are limited to a period of time of more than 20 years ago. For this reason, future work will focus on the application of multi-temporal InSAR techniques to more recent Sentinel-1 data for the monitoring of a larger extent of the communities along the US Atlantic coast.

Data Availability

ERS-1/2 data are provided by ESA through the EOLi-SA (Earth Observation Link) client for Earth Observation Catalogue Service. The SRTM DEM is provided by the United States Geological Survey (USGS) though the EarthExplorer online catalogue (https://earthexplorer.usgs.gov/). LiDAR data of Norfolk (VA) are provided by NOAA Office for Coastal Management (https://coast.noaa.gov).

Funding

This research was partly conducted during S.F. PhD at the Department of Geosciences of the University of Padua, Italy. S.W. thanks the Florida Office of Insurance Regulations for supporting the Miami Beach component of the research. This is contribution number 938 from the Southeast Environmental Research Center in the Institute of Environment at Florida International University.

Author contributions

S.F. carried out the InSAR analysis. S.W. helped with the interpretation of the results. Both authors contributed in the writing of the manuscript.

Data and materials availability

All data needed to evaluate the results and conclusions reported in the paper are present in the main text or in the Supplementary Materials. If necessary, further data may be requested from the authors.

Declaration of competing interest

The authors declare that they have no known competing financial interests or personal relationships that could have appeared to influence the work reported in this paper.

Appendix A. Supplementary data

Supplementary data to this article can be found online at https://doi.org/10.1016/j.ocecoaman.2019.105078.

References

Aerts, J.C.J.H., Botzen, W.J.W., Emanuel, K., Lin, N., de Moel, H., Michel-Kerjan, E.O., 2014. Evaluating flood resilience strategies for coastal megacities. Science 344, 472–474.
Amelung, F., Galloway, D.L., Bell, J.W., Zebker, H.A., Laczniak, R.J., 1999. Sensing the ups and downs of Las Vegas: InSAR reveals structural control of land subsidence and aquifer-system deformation. Geology 27, 483–486.
Bamler, R., Just, D., 1993. Phase statistics and decorrelation in SAR interferograms. In: Geoscience and Remote Sensing Symposium. IGARSS, pp. 980–984.
Bekaert, D.P.S., Hamlington, B.D., Buzzanga, B., Jones, C.E., 2017. Spaceborne synthetic aperture radar Survey of subsidence in Hampton roads, Virginia (USA). Sci. Rep. *7*.
Berardino, P., Fornaro, G., Lanari, R., Sansosti, E., 2002. A new algorithm for surface deformation monitoring based on small baseline differential SAR interferograms. IEEE Trans. Geosci. Remote Sens. 40, 2375–2383.
Bock, Y., Wdowinski, S., Ferretti, A., Novali, F., Fumagalli, A., 2012. Recent subsidence of the Venice Lagoon from continuous GPS and interferometric synthetic aperture radar. Geochem. Geophys. Geosyst. *13*.
Burgos, A.G., Hamlington, B.D., Thompson, P.R., Ray, R.D., 2018. Future nuisance flooding in Norfolk, VA, from astronomical tides and annual to decadal internal climate variability. Geophys. Res. Lett. 45, 12432–12439.
Chaussard, E., Amelung, F., Abidin, H., Hong, S.H., 2013. Sinking cities in Indonesia: ALOS PALSAR detects rapid subsidence due to groundwater and gas extraction. Remote Sens. Environ. 128, 150–161.
Costantini, M., 1998. A novel phase unwrapping method based on network programming. IEEE Trans. Geosci. Remote Sens. 36, 813–821.
Crosetto, M., Monserrat, O., Adam, N., Parizzi, A., Bremmer, C., Dortland, S., Hanssen, R. F., Van Leijen, F.J., 2008. Validation of existing processing chains in TerraFirma stage 2-Final Report. In: GMES TERRAFIRMA ESRIN, p. 15.
Dixon, T.H., Amelung, F., Ferretti, A., Novali, F., Rocca, F., Dokka, R., Sella, G., Kim, S. W., Wdowinski, S., Whitman, D., 2006. Subsidence and flooding in new Orleans. Nature 441, 587–588.
Eggleston, J., Pope, J., 2013. Land subsidence and relative sea-level rise in the southern Chesapeake Bay region. In: U.S. Geological Survey Circular.
Emardson, T.R., Simons, M., Webb, F.H., 2003. Neutral atmospheric delay in interferometric synthetic aperture radar applications: statistical description and mitigation. Journal of Geophysical Research-Solid Earth *108*.
Engelhart, S.E., Horton, B.P., 2012. Holocene sea level database for the Atlantic coast of the United States. Quat. Sci. Rev. 54, 12–25.
Ezer, T., 2013. Sea level rise, spatially uneven and temporally unsteady: why the US East Coast, the global tide gauge record, and the global altimeter data show different trends. Geophys. Res. Lett. 40, 5439–5444.
Galloway, D.L., Burbey, T.J., 2011. Review: regional land subsidence accompanying groundwater extraction. Hydrogeol. J. 19, 1459–1486.
Gatelli, F., Guarnieri, A.M., Parizzi, F., Pasquali, P., Prati, C., Rocca, F., 1994. The wavenumber shift in sar interferometry. IEEE Trans. Geosci. Remote Sens. 32, 855–865.
Goldstein, R.M., Werner, C.L., 1998. Radar interferogram filtering for geophysical applications. Geophys. Res. Lett. 25, 4035–4038.
Hanssen, R.F., 2001. Radar Interferometry: Data Interpretation and Error Analysis. Springer, Dordrecht.
Havazli, E., Wdowinski, S., 2017. The effect of temporal resolution due to atmospheric phase delay on minimum detectable signal in InSAR time series: application to slow deformation over socorro magma body. In: FRINGE. Finland, Helsinki.

Hong, S.H., Wdowinski, S., 2014. Double-bounce component in cross-polarimetric SAR from a new scattering target decomposition. IEEE Trans. Geosci. Remote Sens. 52, 3039–3051.
Karegar, M.A., Dixon, T.H., Engelhart, S.E., 2016. Subsidence along the atlantic coast of north America: insights from GPS and late Holocene relative sea level data. Geophys. Res. Lett. 43, 3126–3133.
Karegar, M.A., Dixon, T.H., Malservisi, R., Kusche, J., Engelhart, S.E., 2017. Nuisance flooding and relative sea-level rise: the importance of present-day land motion. Sci. Rep. *7*.
Kemp, A.C., Bernhardt, C.E., Horton, B.P., Kopp, R.E., Vane, C.H., Peltier, W.R., Hawkes, A.D., Donnelly, J.P., Parnell, A.C., Cahill, N., 2014. Late Holocene sea- and land-level change on the US southeastern Atlantic coast. Mar. Geol. 357, 90–100.
Kim, S.W., Wdowinski, S., Dixon, T.H., Amelung, F., Won, J.S., Kim, J.W., 2008. InSAR-based mapping of surface subsidence in Mokpo City, Korea, using JERS-1 and ENVISAT SAR data. Earth Planets Space 60, 453–461.
Kirshen, P., Knee, K., Ruth, M., 2008. Climate change and coastal flooding in Metro Boston: impacts and adaptation strategies. Clim. Change 90, 453–473.
Kleinosky, L.R., Yarnal, B., Fisher, A., 2007. Vulnerability of Hampton Roads, Virginia to storm-surge flooding and sea-level rise. Nat. Hazards 40, 43–70.
Lane, E. (Ed.), 1994. Florida's Geological History and Geological Resources Special Publication No. 35. Department of Environmental Protection, Florida Geological Survey, Tallahassee, FL.
Nikitina, D., Kemp, A.C., Engelhart, S.E., Horton, B.P., Hill, D.F., Kopp, R.E., 2015. Sea-level change and subsidence in the Delaware Estuary during the last-2200 years. Estuar. Coast Shelf Sci. 164, 506–519.
Osmanoglu, B., Dixon, T.H., Wdowinski, S., Cabral-Cano, E., Jiang, Y., 2011. Mexico City subsidence observed with persistent scatterer InSAR. Int. J. Appl. Earth Obs. Geoinf. 13, 1–12.
Poitevin, C., Woppelmann, G., Raucoules, D., Le Cozannet, G., Marcos, M., Testut, L., 2019. Vertical land motion and relative sea level changes along the coastline of Brest (France) from combined space-borne geodetic methods. Remote Sens. Environ. 222, 275–285.
Sarmap, 2014. SARscape 5.1 help. Available online at: https://www.harrisgeospatial.com/docs/pdf/sarscape_5.1_help.pdf.
Sella, G.F., Stein, S., Dixon, T.H., Craymer, M., James, T.S., Mazzotti, S., Dokka, R.K., 2007. Observation of glacial isostatic adjustment in "stable" North America with GPS. Geophys. Res. Lett. *34*.
Seymour, M.S., Cumming, I.G., 1994. Maximum likelihood estimation for SAR interferometry. In: Proceedings of IGARSS '94 - 1994 IEEE International Geoscience and Remote Sensing Symposium, pp. 2272–2275 (Pasadena, CA, USA).
Solano-Rojas, D., Wdowinski, S., Cabral-Cano, E., Osmanoğlu, B., 2019. Geohazard assessment of Mexico City's Metro System derived from SAR interferometry observations. Science Advances. Submitted for publication.
Strang, G., 1988. Linear Algebra and its Appications. Orlando, FL, USA.
Wdowinski, S., Bray, R., Kirtman, B.P., Wu, Z.H., 2016. Increasing flooding hazard in coastal communities due to rising sea level: case study of Miami Beach, Florida. Ocean Coast Manag. 126, 1–8.
Yamaguchi, Y., Moriyama, T., Ishido, M., Yamada, H., 2005. Four-component scattering model for polarimetric SAR image decomposition. IEEE Trans. Geosci. Remote Sens. 43, 1699–1706.
Zervas, C.E., 2009. Sea Level Variations of the United States. NOAA Technical Report NOS CO-OPS 053, pp. 1854–2006.